

Lawrence Berkeley National Laboratory

LBL Publications

Title

Broadband (0-4 Hz) Ground Motions for a Magnitude 7.0 Hayward Fault Earthquake With Three-Dimensional Structure and Topography

Permalink

<https://escholarship.org/uc/item/7np1s397>

Journal

Geophysical Research Letters, 45(2)

ISSN

0094-8276

Authors

Rodgers, Arthur J
Pitarka, Arben
Petersson, N Anders
[et al.](#)

Publication Date

2018-01-28

DOI

10.1002/2017gl076505

Peer reviewed

RESEARCH LETTER

10.1002/2017GL076505

Key Points:

- Efficient high-performance computing simulations greatly increase ground motion frequencies of a Hayward Fault earthquake
- Path effects result in higher motions on the eastern side of the fault compared to the western side
- Simulated intensities are consistent with Ground Motion Prediction Equations, but path and site effects for the 3D model lead to greater scatter

Supporting Information:

- Supporting Information S1

Correspondence to:

A. J. Rodgers,
rodders7@llnl.gov

Citation:

Rodgers, A. J., Pitarka, A., Petersson, N. A., Sjögreen, B., & McCallen, D. B. (2018). Broadband (0–4 Hz) ground motions for a magnitude 7.0 Hayward fault earthquake with three-dimensional structure and topography. *Geophysical Research Letters*, 45, 739–747. <https://doi.org/10.1002/2017GL076505>

Received 21 NOV 2017

Accepted 3 JAN 2018



Accepted article online 8 JAN 2018

Published online 30 JAN 2018

©2018. The Authors.

This is an open access article under the terms of the Creative Commons Attribution-NonCommercial-NoDerivs License, which permits use and distribution in any medium, provided the original work is properly cited, the use is non-commercial and no modifications or adaptations are made.

Broadband (0–4 Hz) Ground Motions for a Magnitude 7.0 Hayward Fault Earthquake With Three-Dimensional Structure and Topography

Arthur J. Rodgers^{1,2,3} , Arben Pitarka¹, N. Anders Petersson⁴ , Björn Sjögreen⁴, and David B. McCallen^{2,5}

¹Atmospheric, Earth and Energy Division and Geophysical Monitoring Program, Lawrence Livermore National Laboratory, Livermore, CA, USA, ²Energy Geosciences Division, Lawrence Berkeley National Laboratory, Berkeley, CA, USA, ³Berkeley Seismological Laboratory, University of California, Berkeley, CA, USA, ⁴Center of Applied Scientific Computing, Lawrence Livermore National Laboratory, Livermore, CA, USA, ⁵Office of the President, University of California, Oakland, CA, USA

Abstract We performed fully deterministic broadband (0–4 Hz) high-performance computing ground motion simulations of a magnitude 7.0 scenario earthquake on the Hayward Fault (HF) in the San Francisco Bay Area of Northern California. Simulations consider average one-dimensional (1-D) and three-dimensional (3-D) anelastic structure with flat and topographic free surfaces. Ground motion intensity measures (GMIMs) for the 3-D model display dramatic differences across the HF due to geologic heterogeneity, with low wave speeds east of the HF amplifying motions. The median GMIMs agree well with Ground Motion Prediction Equations (GMPEs); however, the 3-D model generates more scatter than the 1-D model. Ratios of 3-D/1-D GMIMs from the same source allow isolation of path and site effects for the 3-D model. These ratios show remarkably similar trends as site-specific factors for the GMPE predictions, suggesting that wave propagation effects in our 3-D simulations are on average consistent with empirical data.

Plain Language Summary With the use of powerful supercomputers and an efficient numerical method, modeling of ground shaking for a magnitude 7.0 earthquake on the Hayward Fault results in more realistic motions than previously achieved. The model includes the current best representation of the Earth (geology and surface topography) to compute seismic wave ground shaking throughout the region. Shaking intensity shows differences across the Hayward Fault that arise from rocks of different geologic origin. On average, results are consistent with models based on actual recorded earthquake motions from around the world. This study shows that powerful supercomputing can be used to calculate earthquake shaking with more realism than previously obtained.

1. Introduction

The Hayward Fault (HF) is a major strike-slip fault on the eastern side of the San Francisco Bay Area (SFBA). This fault is capable of magnitude (M) 7 earthquakes and presents significant ground motion hazard to the heavily populated “East Bay” including the cities of Oakland, Berkeley, Hayward, and Fremont. The HF last ruptured in 1868 with an M 6.8–7.0 event (e.g., Topozada et al., 2002). Instrumental observations of this earthquake are not available; however, historical triangulation data inform the seismic moment and fault length (Yu & Seagall, 1996). Reported intensities were used to create a ShakeMap for the 1868 event (Boatwright & Bundock, 2008). Modified Mercalli Intensities of XIII–IX were experienced near the HF and associated with structural damage. Currently, the HF represents the most likely fault in the San Francisco Bay Area (SFBA) to rupture with an M 6.7 or greater in the next 30 years according to the Uniform California Earthquake Rupture Forecast, Version 3 (Field et al., 2015). A repeat of the 1868 earthquake would cause wide spread damage to structures and transportation and utility lifelines, as well as economic and social disruption.

Estimating ground shaking from damaging earthquakes is central to seismic hazard analysis. Near-fault ground motions (seismograms) and ground motion intensity measurements (GMIMs) are shaped by details of the earthquake rupture, such as the distribution of slip, risetime, rupture speed, and directivity as well as velocity pulses and displacement steps. Ground Motion Prediction Equations (GMPEs) such as those developed by the Pacific Earthquake Engineering Research Center Next Generation Attenuation project provide

empirical models for estimating ground motions. However, these models are based on relatively few recordings of large earthquakes in the critical near-fault region (<20 km) from worldwide recordings and are biased by specific geologic conditions and rupture details of each recording. Consequently, physics-based numerical simulation of ground motions using region-specific fault geometry and geologic structure offers an attractive alternative to reliance on empirical models. Ground motion simulations of large earthquakes are gaining acceptance as computational methods improve, computing resources become more powerful, and representations of three-dimensional (3-D) Earth structure and earthquake sources become more realistic (Aagaard et al., 2008, 2010; Cui et al., 2013; Graves et al., 2008; Olsen et al., 2008).

Importantly, physics-based time domain simulations include 3-D wave propagation to capture complex path and site effects (e.g., Asano et al., 2016; Bielak et al., 2010; Chaljub et al., 2010; Day et al., 2008; Frankel et al., 2009; Taborda & Bielak, 2013) that are not included in stochastic methods (Boore, 1983). In fact, understanding and reducing the scatter in GMIMs due to path and site effects remain a goal in 3-D simulation studies. For simulations to provide motions for time domain engineering analysis of structures, they must resolve the highest possible frequencies, up to several (5–10) Hz or higher. This requires fine spatial discretization of 2–10 m, and large ruptures can span 100 km or more. Consequently, computational domains must include tens to hundreds of billions of points that require massively parallel computers to run simulations for relevant frequencies. Note also that low frequencies and static displacements (corresponding to zero frequency) are important for near-fault seismic hazard and are directly represented in physics-based ground motion simulations.

While many 3-D ground motion simulation studies have focused on Southern California, Northern California has received less attention. Previous work simulated low-frequency ground motions (≤ 1 Hz) using a 3-D model from the United States Geological Survey (USGS, 2017) (Aagaard et al., 2008; Harmsen et al., 2008; Larsen et al., 2000). An updated version of this model (USGS, 2017) is the current best representation of 3-D structure for seismic simulations. Aagaard et al. (2010, including coauthors of this study) performed the most comprehensive study of HF scenarios to date, considering 39 ruptures. They reported motions from 3-D simulations from various groups up to 1 Hz and hybrid simulations up to 10 Hz. Recently, Johansen et al. (2017) reported a 2.5 Hz simulation of HF earthquake ground motions. Doubling the frequency requires 16 times greater computational effort; consequently, increasing the resolution of full waveform simulations is nontrivial.

We report simulations of ground motions for an M 7 earthquake on the HF including frequencies from static displacements to 4 Hz and using average plane-layered one-dimensional (1-D) and 3-D USGS anelastic Earth models with surface topography. In order to efficiently achieve such high resolution, simulations used mesh refinement and significant allocations of high-performance computing. Consideration of 1-D and 3-D models allows us to quantify path and site effects from the 3-D model. We found dramatic differences in shaking intensity across the HF and attribute this to path and site effects arising from heterogeneity in the Earth model. Computed GMIMs are consistent with median GMPE values (Abrahamson et al., 2014), and path and site effects from 3-D structure result in larger scatter than the 1-D model. We isolate path and site effects by forming 3-D/1-D GMIM ratios with the same source. While the veracity of these path effects across the HF remains the subject of future investigations using recorded motions from actual events, the analysis presented herein can provide insight to ground motion hazard in the near-fault region and new ground motions for seismic hazard and risk analysis in the SFBA.

2. SW4 Simulations

SW4 (Seismic Waves, fourth order) is a fourth order in space and time finite difference code for seismic wave simulations on large, distributed memory, parallel computers. It uses piecewise structured Cartesian and curvilinear grids to discretize the governing equations based on the principle of summation-by-parts (SBP), leading to a provably energy stable numerical method. SW4 includes several important features for accurate and efficient simulations of seismic waves, including surface topography, attenuation, and mesh refinement (Pettersson & Sjogreen, 2012, 2014; 2015; Sjogreen & Pettersson, 2012). Surface topography is represented on a curvilinear grid that SW4 generates automatically based on a user-supplied relief. SW4 evolved from Wave Propagation Project (a second-order SBP code), which has been used in previous SFBA ground motion simulation studies (Aagaard et al., 2008, 2010; Rodgers et al., 2008). SW4 supports mesh refinement with

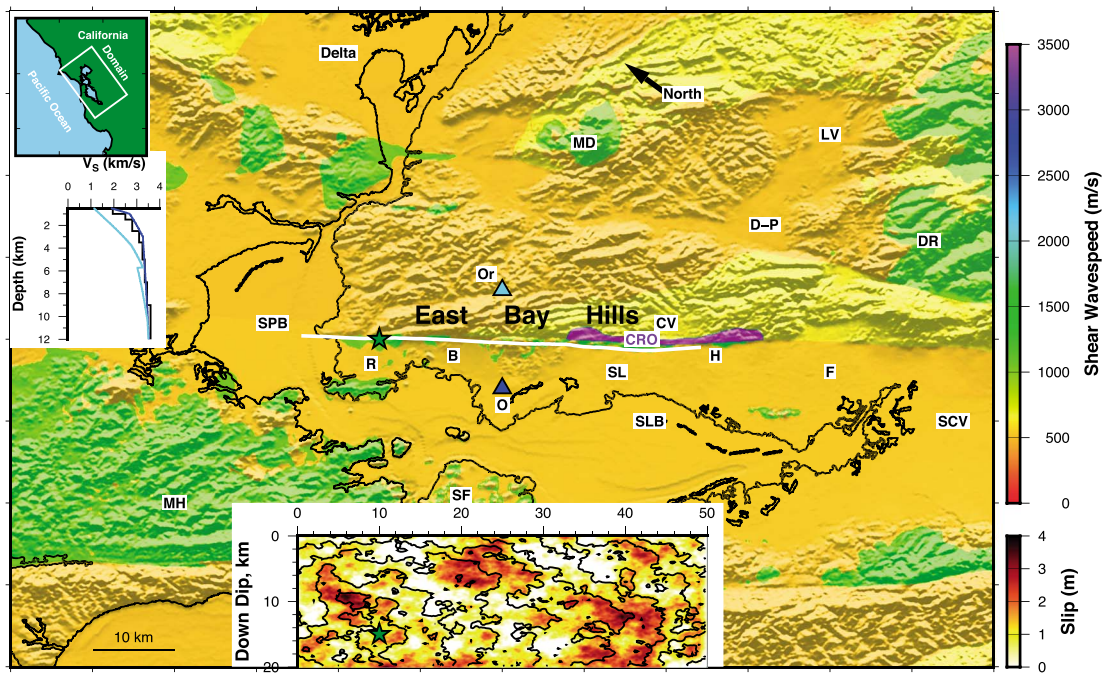


Figure 1. Computational domain covering the central San Francisco Bay Area and showing the shear wave speed (v_s) at the surface (color bar) and topographic relief. Also shown are the extent of the HF rupture (white line) and locations/features mentioned in the text (SPB = San Pablo Bay, R = Richmond, B = Berkeley, Or = Orinda, O = Oakland, CRO = Coast Ranges Ophiolite, SL = San Leandro, SLB = San Leandro Basin, CV = Castro Valley, H = Hayward, F = Fremont, D-P = Dublin-Pleasanton, LV = Livermore Valley, DR = Diablo Range, MD = Mount Diablo, SCV = Santa Clara Valley, MH = Marin Highlands). (top left inset) Orientation map showing domain in map view. (left inset) V_s profiles at Orinda (cyan) and Oakland (blue) along with the 1-D model (black). (bottom inset) Slip distribution for the rupture model plotted parallel to the HF, along with hypocenter (green star) and time-to-rupture contours (2 s intervals).

hanging nodes. Compared to using a constant grid size, mesh refinement significantly reduces the total number of grid points. It can also allow a maximal time step without violating the Courant-Friedrichs-Lewy condition for convergence (Courant et al., 1928; Petersson et al., 2017). SW4 and the SPECFEM3D spectral element method codes (Peter et al., 2011) are broadly similar in that they allow the mesh to coarsen with depth as wave speeds increase.

We considered a computational domain spanning the central SFBA, centered on the HF. The 1-D and 3-D simulations had a minimum shear wave speed (V_s) of 700 and 500 m/s, respectively. The near-surface V_s values from the 3-D model are as low as 200 m/s, especially on the eastern shore of the San Francisco Bay. However, these near-surface layers are often thin and tend to be underlain by stronger materials ($V_s > 500$ m/s). Such low wave speeds require even more computational resources to resolve frequencies to 4 Hz. A minimum V_s of 500 m/s is a reasonable and practical compromise for the purposes of the simulation considered herein. Furthermore, nonlinear response to large ground motions can become important for weak soils and is beyond the scope of this study. Our simulations resolved frequencies from static displacements to 4 Hz. We computed the three-component velocity seismograms (90 s) on a dense grid of points spanning the domain with 2 km spacing (supporting information).

Figure 1 shows the computational domain (dimensions 120 × 80 km at the surface, 30 km depth) with surface V_s for the 3-D model. Surface V_s values are relatively low (500–700 m/s), except the very high V_s body (Coast Range Ophiolite, CRO) along the HF near Castro Valley and the topographic highs (Mount Diablo, Diablo Range, and Marin Highlands). The fault extent is also shown, spanning Point Pinole in the north to Hayward in the south. The fault surface follows the nonplanar geometry in the USGS model, although we also considered a planar vertical fault (supporting information). The slip distribution is shown along with the hypocenter, near Richmond. The rupture model was generated following the method of Graves and Pitarka (2010, 2015, 2016 (GP16)) (supporting information). The GP16 rupture model was tested and validated against recorded data as part of the Southern California Earthquake Center Broadband Platform (Dreger et al.,

2015; Goulet et al., 2015). Among several rupture realizations, we chose this particular slip distribution because it has little shallow slip in the northern extent (Berkeley to the north) and south of Oakland, where geodetic analysis infers creep along the fault (Chaussard et al., 2015). The point of this study is not to forecast the specifics of an M 7 HF earthquake, but rather to demonstrate that fully deterministic 3-D simulations with frequencies up to 4 Hz are possible, to compare motions with GMPEs, and to investigate the impact of path and site effects on ground motions.

We considered three simulations in this study, each with the same rupture model, but with different Earth models. These are a 1-D model with a flat free surface (*1DFLAT*), the 3-D USGS model with a flat free surface (*3DFLAT*), and the 3-D USGS model with a topographic free surface (*3DTOPO*) (see the supporting information). The 1-D model (Kamai et al., 2014) is representative of the SFBA region; however, we modified the near-surface wave speeds to have 30 m slowness-averaged wave speed (V_{S30}) of 886 m/s. Geological heterogeneity across the HF is reflected in strong differences in wave speeds in the USGS 3-D model. The rocks west of the HF are predominantly Franciscan Complex, while the East Bay Hills east of the HF are of the sedimentary Great Valley Complex (Graymer et al., 2005). Material properties in the USGS 3-D model were assigned based on rules developed from empirical measurements, and these result in much lower upper crustal wave speeds for the Great Valley Complex than the Franciscan Complex (Brocher, 2005). An inset in Figure 1 shows the V_S profiles to 12 km below sea level for the 1-D and 3-D models at points in Oakland and Orinda. The 1-D and 3-D model in Oakland are very similar. However, V_S is substantially lower in the East Bay Hills and Great Valley Complex compared to Oakland. Topography across the domain is significant, with the highest point (Mount Diablo) at over 1,170 m and bathymetry to 90 m below sea level.

3. Results

The simulations described above provide seismograms of ground motions for an M 7.0 HF earthquake throughout the SFBA. As expected the motions are large near the fault with peak ground accelerations (PGA) and peak ground velocities (PGV) of ~ 1 g and ~ 1 m/s, respectively, and capable of damage to the built environment (e.g., buildings, roads, and bridges). Figure 2 shows map views of the PGV for two cases. The *1DFLAT* case (Figure 2a) shows the expected nearly symmetrical pattern of PGV across a nearly vertical fault in a 1-D model and forward directivity to the south (positive x direction, right). Symmetry is broken by the nonplanar geometry of the fault and variations in rake. The largest PGVs are seen above the asperities.

The *3DTOPO* case (Figure 2b) shows a much more complex pattern of motions that combine source, 3-D path, and site effects. Four features are most noteworthy. First, motions are stronger in the East Bay Hills (Great Valley Complex) where upper crustal shear wave speeds are lower compared to areas on the west side of the HF. Specifically, a broad region east of the HF and outside the CRO (e.g., Orinda and Castro Valley) has higher PGVs than locations west of the HF (e.g., Berkeley, Oakland, and San Leandro). We attribute this to lower V_S in the upper crust on the Great Valley Complex on the eastern side. Second, the high V_S along the eastern side of the HF near Castro Valley associated with the CRO (Figure 1) result in lower ground motions within the body and higher motions around the edges. Third, the 3-D cases show strong shaking in the sedimentary basins of eastern San Pablo Bay, the Sacramento-San Joaquin Delta, San Leandro Basin, Dublin-Pleasanton, Livermore, and Santa Clara Valleys. Fourthly, the higher V_S mountainous areas of Mount Diablo, the Diablo Range, and the Marin Highlands (Figure 1) experience lower PGVs than surrounding areas. The supporting information includes figures showing PGV for different cases.

In order to evaluate path effects, we also show the natural logarithm ratio of the *3DTOPO/3DFLAT* in Figure 2c. This quantifies the effects of surface topography and shows that motions are amplified on peaks and along ridges consistent with previous reports (e.g., Lee et al., 2009), while flat areas show little or no amplitude differences. The effect of 3-D structure is seen in the natural logarithm ratio of *3DTOPO/1DFLAT* shown in Figure 2d. Here large amplification, as much as $2\times$ (0.7 ln units), is seen in the East Bay Hills and eastern San Pablo Bay, while lower motions are seen west of the Hayward Fault in Berkeley, Oakland, and San Leandro and in the Coast Range Ophillite.

To assess the consistency of our simulations with empirical data, we compared GMIMs to GMPEs. Figures 3a–3c show the PGV versus Joyner-Boore distance for three Earth models. Each point represents a measurement from a hypothetical dense network of stations with 2 km spacing. Symbols indicate locations east (squares) or

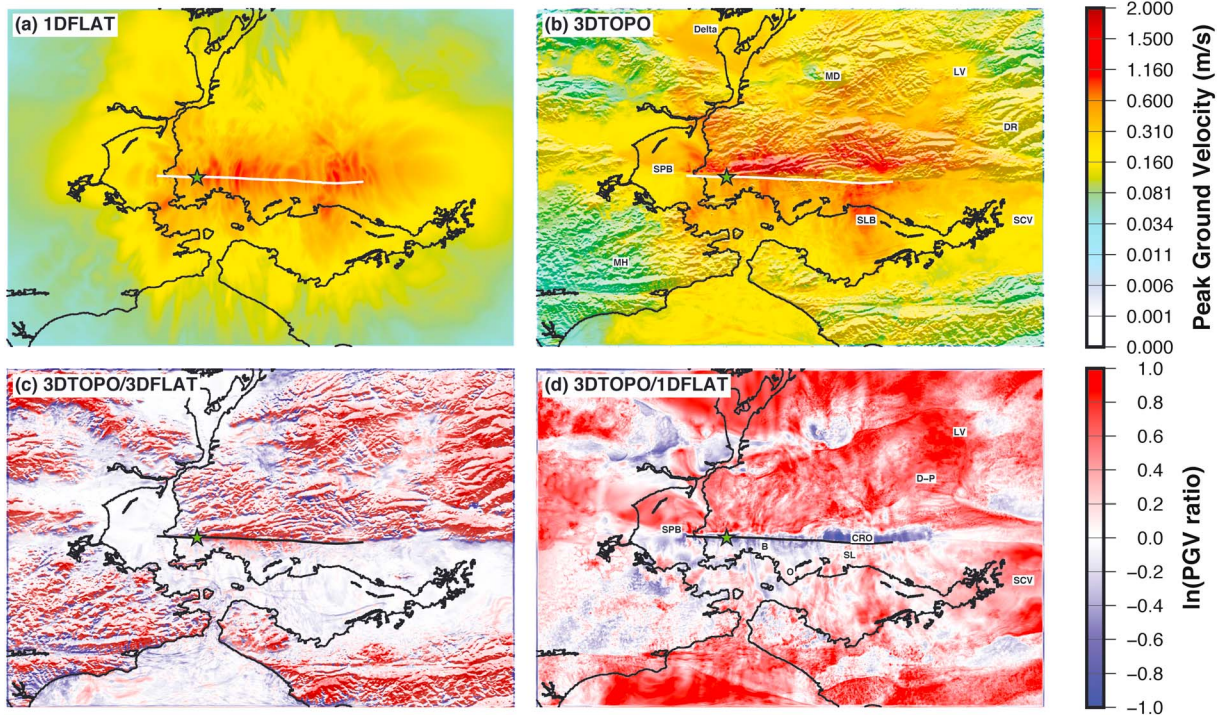


Figure 2. Peak ground velocity (PGV) in map view across the computational domain according to the color scale (white-red) for the (a) *1DFLAT* and (b) *3DTOPO* cases. Natural logarithm ratio of PGV for (c) *3DTOPO/3DFLAT* and (d) *3DTOPO/1DFLAT* plotted according to the color scale (blue-red). The surface projection of the Hayward Fault rupture is shown in Figures 2a and 2b by the white line and in Figures 2c and 2d by the black line. Place names are the same as Figure 1.

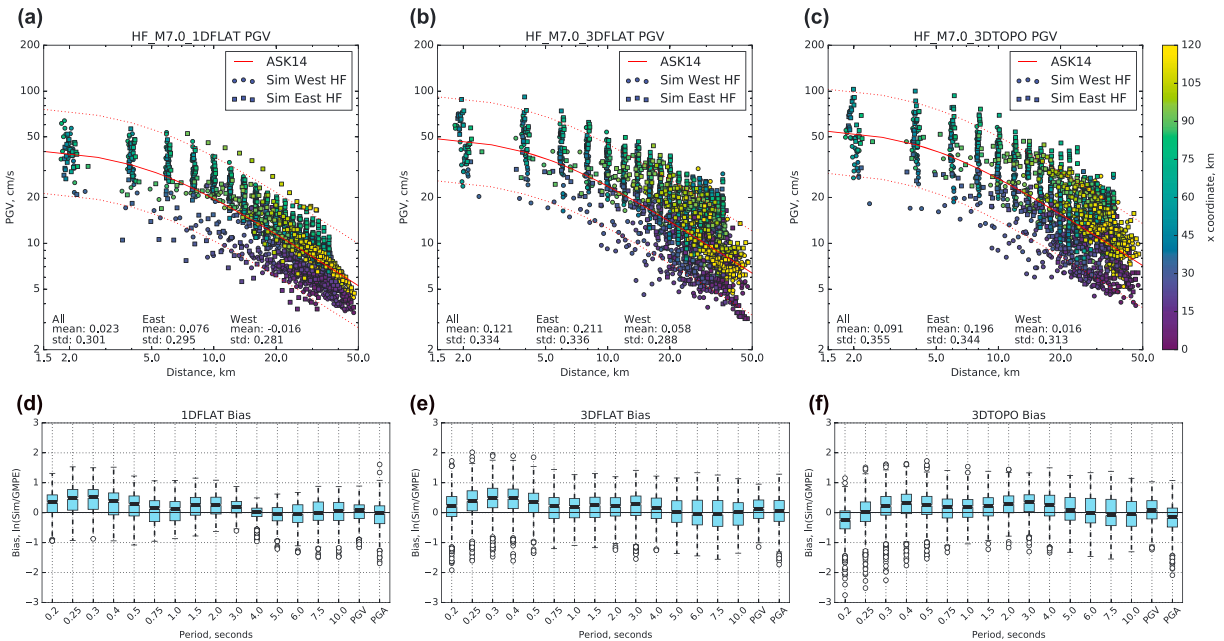


Figure 3. Peak ground velocity (PGV) versus distance for the three cases: (a) *1DFLAT*, (b) *3DFLAT*, and (c) *3DTOPO*. Points east and west are shown as squares and circles, respectively, and are color-coded by the x coordinate to indicate directivity effects. The GMPE prediction from Abrahamson et al. (2014; ASK14) and its spread are shown as red solid and dashed lines, respectively. Summary statistics of the bias (mean and standard deviation) for all points and those east and west of the HF are given in each panel. Boxplots of RotD50 spectral acceleration (S_a), PGV and PGA bias (see text) for three Earth models: (d) *1DFLAT*, (e) *3DFLAT*, and (f) *3DTOPO*. The box indicates two central quartiles (25–75%) and the median (thick line). The whiskers indicate 1.5 times the interquartile range (IQR), and the circles show outliers (points beyond 1.5IQR).

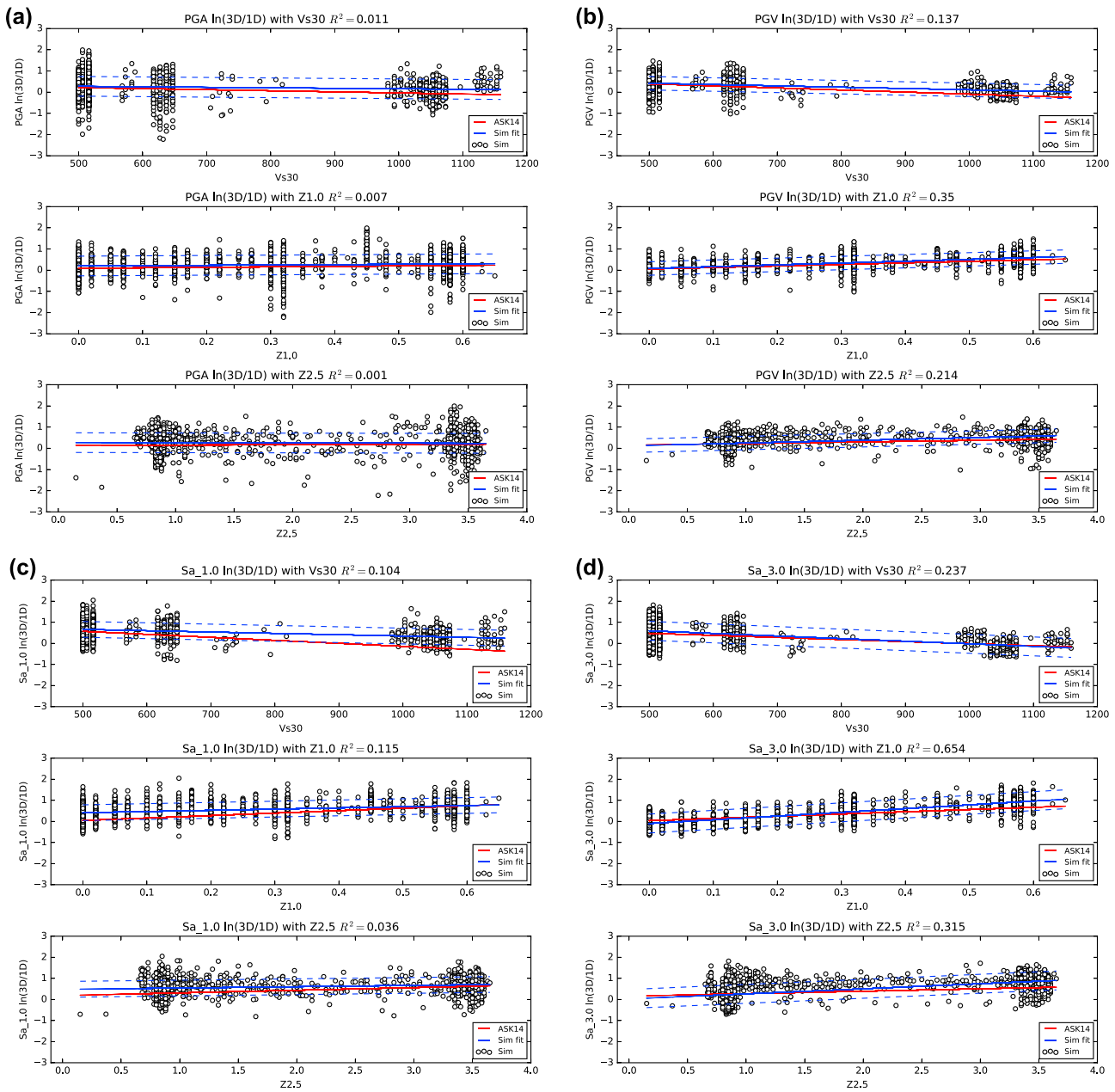


Figure 4. Path and site bias (natural logarithm of 3D/1D) GMIM for each site (circles) plotted against site-specific terms Vs30, Z1.0 and Z2.5; specific GMIMs are (a) PGA, (b) PGV, and (c) Sa_{1.0} and (d) Sa_{3.0}. In each panel, a linear regression model is plotted (blue line, 1σ error as dashed blue) with coefficient of determination (R²) given in the panel title. Predictions of the bias from the ASK14 GMPE are shown as the red lines.

west (circles) of the HF and are color-coded by the x coordinate to indicate forward directivity in the positive x direction (southeast). The GMPE predictions (Abrahamson et al., 2014; ASK14) versus distance are made for average path and site properties. Statistics summarizing the bias (natural logarithm of the ratio simulation/GMPE) using the site-specific GMPE predictions are given for each case (Vs30, and Z1.0 and Z2.5, the depth to V_s of 1.0 and 2.5 km/s, respectively). All cases show stronger/weaker motions in the forward/backward directivity (larger/smaller x). The PGV values for the 1D/FLAT model (Figure 3a) are consistent with the GMPE model with mean bias near zero as is expected from the GP16 method. Locations east and west of HF for the 1D/FLAT case show little difference in the mean values (bias less than 0.092 or ~10%) as expected from near symmetry across the HF. Cases with the 3-D Earth model (3D/FLAT

and *3D*TOPO) show more variation than the *1D*FLAT model; however, on average, the simulated values have near-zero mean bias (0.121 and 0.091, respectively) indicating that the simulated PGVs are consistent with the median GMPE predictions. The mean PGV values for the *3D*TOPO model are 20% (0.18 natural log units) higher for the entire east side of the HF compared to the entire west side. Figure 2d shows that for sites near the fault the amplitudes are as much as a factor of 2 larger in the Great Valley Complex compared to mirror image sites across the HF.

We also compared the median horizontal component response spectra (RotD50) from our simulations to GMPE predictions. Figures 3d–3f show the bias (natural logarithm of the ratio simulation/GMPE) across periods from 0.2 to 10 s (0.1 to 5 Hz) for the three Earth models. Note that we could not resolve the shortest periods in this range and that the response spectra are sensitive to motions about $\pm 25\%$ of the target period. Also shown are the PGV and PGA bias. In each case we use the site-specific GMPE parameters for each location. The *1D*FLAT case shows near-zero bias across all resolved periods and the least scatter of the three cases. The median biases are slightly high (~ 0.5) for the 0.25–0.5 s samples for the *1D*FLAT and *3D*FLAT cases. All median values fall within ± 0.7 log units, which is typical for the standard deviation of the GMPE predictions. Finally, there is larger variance and more outliers for the *3D*TOPO case suggesting that path and site effects due to 3-D structure and topography cause more variation in the ground motions than is captured by the GMPEs. This scatter (up to 2 log units) is significantly higher than the uncertainties from the GMPEs.

Our simulations with 1-D and 3-D models and with the same source enable differential measurements to isolate path and site effects from the 3-D Earth structure. We formed ratios of the 3-D/1-D GMIMs at each site and correlated these with site-specific terms: V_{s30} , and $Z_{1.0}$ and $Z_{2.5}$. Linear regression models were calculated to determine if variability in GMIMs can be explained by these site terms and were compared with GMPE predictions. Figure 4 shows this 3-D/1-D bias as the natural logarithm of the GMIM ratio (*3D*TOPO/*1D*FLAT) for PGA, PGV, and RotD50 spectral values for 1.0 and 3.0 s plotted against the three site-specific terms. In each panel, the 3-D/1-D bias is regressed against the site term and we show the resulting best fit line, errors, and coefficient of determination (R^2).

The 3-D/1-D bias for PGA is poorly correlated ($R^2 \sim 0$) with all three site terms, indicating that the large variability cannot be explained with these site terms. The 3-D/1-D biases for PGV, $Sa_{1.0}$ and $Sa_{3.0}$ are negatively correlated with V_{s30} as expected, but correlations are quite weak. Also, V_{s30} values in our simulations were limited to 500 m/s or higher. The V_{s30} values cluster around 500–650 and 950–1,150 m/s, and we discarded the points on the CRO ($V_{s30} \sim 3,500$ m/s). Stronger positive correlations ($R^2 > 0.2$) are seen for longer period motions PGV and $Sa_{3.0}$ with $Z_{1.0}$ and $Z_{2.5}$, indicating that ground motion amplitudes increase for deeper low shear wave speeds as expected in basins. We also show the same ratios for the ASK14 GMPE predictions in Figure 4. The trends of the regression fits and the GMPE predictions are remarkably similar and within the regression errors. This indicates that our simulations can independently reproduce the median path and site effects in the empirical data as represented by the ASK14 GMPE model. Understanding the physical basis of variability due to path and site effects remains an important goal of physics-based simulations and will require further investigation.

4. Discussion and Conclusions

This study reports simulated ground motions for an $M 7$ scenario earthquake on the Hayward Fault using 3-D Earth structure and surface topography spanning frequencies from static displacements to 4 Hz. It represents the highest resolution regional-scale 3-D ground motion simulations performed to date for damaging earthquakes in Northern California. This effort was made possible with the advances in numerical methods that underlie the SW4 code and significant HPC resources. Results show that the GP16 earthquake source rupture model and our SW4 wave propagation simulations for both the 1-D and 3-D models generate motions that are consistent with the median GMPE predictions and that the trends in 3-D/1-D bias are remarkably consistent with the ASK14 GMPE (Figures 3 and 4). This gives us confidence that the ground motions are consistent with the average behavior observed in nature.

Simulations with the USGS 3-D model of the SFBA show dramatic effects of path propagation and site response. In particular, the high ground motion intensities in the East Bay Hills should be of concern for residents and the larger community that relies on the infrastructure located therein. For example, Highway 13; the Caldecott Tunnel (Highway 24); Bay Area Rapid Transit; Interstates 80, 580, and 680; and other

transportation routes as well as utility and water infrastructure (reservoirs and pipelines) are within or near the region of high ground motions (PGV \sim 1 m/s). Steep topography of the East Bay Hills along with strong shaking potentially presents landslide hazards, and this could be a factor for transportation routes.

While this study provides clear evidence that strong ground motions from a Hayward Fault rupture will pose significant risk to structures near the fault, it should be noted that this is only one realization of many possibilities. There are many factors that impact ground motions, particularly details of the rupture such as the slip distribution, rupture speed, risetime, the depth of top of the rupture, the hypocenter (which controls directivity), and coupling of source properties with details of Earth structure, particularly sedimentary basins. Future investigations will hopefully sample diverse rupture scenarios and allow isolation of systematic path and site effects. These will become easier as numerical and computational efficiency improve and we have access to more powerful computational resources. Finally, the Earth structure used in this study is uncertain and the current USGS 3-D model must be evaluated and improved using recordings of moderate events. Some work has been done on this problem (e.g., Kim et al., 2010; Rodgers et al., 2008). Further work is needed to improve waveform predictions through full waveform modeling and inversions with moderate earthquakes.

Acknowledgments

This research was supported by the Exascale Computing Project (ECP), project 17-SC-20-SC, a collaborative effort of two DOE organizations—the Office of Science and the National Nuclear Security Administration. Simulations were performed using a Computing Grand Challenge allocation on Quartz at Lawrence Livermore National Laboratory and with an allocation on Cori Phase-2 at National Energy Research Scientific Computing Center (NERSC), Lawrence Berkeley National Laboratory. SW4 is an open source seismic simulation code developed at LLNL and distributed by the Computational Infrastructure for Geodynamics. Data were processed and plotted using ObsPy (Krischer et al., 2015) and Generic Mapping Tool (Wessel et al., 2013). Response spectra and GMPEs were computed with the pyrotd and pygmm software, respectively, from Albert Kottke (<https://github.com/arkottke>). We used pySW4, from Shahar Shani-Kadmiel to query Z1.0 and Z2.5 from the 3-D model (<https://github.com/shahar-kadmiel/pySW4>). Waveforms for the 1D FLAT and 3D TOPO simulations will be made available upon publication. Comments by Doug Dreger, Mike Pasyanos, Brad Aagaard, and Peggy Hellweg improved the presentation, as did peer reviews by Carl Tape and an anonymous referee. This work was performed under the auspices of the U.S. Department of Energy by LLNL under contract DE-AC52-07NA27344 (LLNL-JRNL-741500).

References

- Aagaard, B. T., Brocher, T. M., Dolenc, D., Dreger, D., Graves, R. W., Harmsen, S., ... Zoback, M. L. (2008). Ground-motion modeling of the 1906 San Francisco earthquake, Part II: Ground-motion estimates for the 1906 earthquake and scenario events. *Bulletin of the Seismological Society of America*, 98(2), 1012–1046. <https://doi.org/10.1785/0120060410>
- Aagaard, B. T., Graves, R. W., Rodgers, A., Brocher, T. M., Simpson, R. W., Dreger, D., ... Jachens, R. C. (2010). Ground motion modeling of Hayward fault scenario earthquakes, Part II: Simulation of long-period and broadband ground motions. *Bulletin of the Seismological Society of America*, 100(6), 2945–2977. <https://doi.org/10.1785/0120090379>
- Abrahamson, N., Silva, W., & Kamai, R. (2014). Summary of the ASK14 ground motion relation for active crustal regions. *Earthquake Spectra*, 30(3), 1025–1055. <https://doi.org/10.1193/070913EQS198M>
- Asano, K., Sekiguchi, H., Iwata, T., Yoshimi, M., Hayashida, T., Saomoto, H., & Horikawa, H. (2016). Modelling of wave propagation and attenuation in the Osaka sedimentary basin, western Japan, during the 2013 Awaji Island earthquake. *Geophysical Journal International*, 204(3), 1678–1694. <https://doi.org/10.1093/gji/ggv543>
- Bielak, J., Graves, R. W., Olsen, K. B., Taborda, R., Ramírez-Guzmán, L., Day, S. M., ... Juve, G. (2010). The ShakeOut earthquake scenario: Verification of three simulation sets. *Geophysical Journal International*, 180(1), 375–404. <https://doi.org/10.1111/j.1365-246X.2009.04417.x>
- Boatwright, J., & Bundock, H. (2008). Modified Mercalli intensity maps for the 1868 Hayward earthquake plotted in ShakeMap format, U.S. Geological Survey Open-File Report 2008–1121
- Boore, D. (1983). *Bulletin of the Seismological Society of America*, 73(6), 1865–1894.
- Brocher, T. (2005). Compressional and shear wave velocity versus depth in the San Francisco Bay Area, California: Rules for USGS Bay Area Velocity Model 05.0.0, United States Geological Survey Open-File Report 05–13172005 (58 p.).
- Chaljub, E., Moczo, P., Tsuno, S., Bard, P.-Y., Kristek, J., Käser, M., ... Kristekova, M. (2010). Quantitative comparison of four numerical predictions of 3D ground motion in the Grenoble Valley, France. *Bulletin of the Seismological Society of America*, 100(4), 1427–1455. <https://doi.org/10.1785/0120090052>
- Chaussard, E., Bürgmann, R., Fattahi, H., Johnson, C. W., Nadeau, R., Taira, T., & Johanson, I. (2015). Interseismic coupling and refined earthquake potential on the Hayward-Calaveras fault zone. *Journal of Geophysical Research: Solid Earth*, 120, 8570–8590. <https://doi.org/10.1002/2015JB012230>
- Courant, R., Friedrichs, K., & Lewy, H. (1928). Über die partiellen Differenzgleichungen der mathematischen Physik. *Mathematische Annalen (in German)*, 100(1), 32–74. <https://doi.org/10.1007/BF01448839>
- Cui, Y., Poyraz, E., Olsen, K. B., Zhou, J., Withers, K., Callaghan, S., ... Jordan, T. H. (2013). Physics-based seismic hazard analysis on petascale heterogeneous supercomputers. In *Proceedings of SC13: International Conference for High Performance Computing, Networking, Storage and Analysis*. <https://doi.org/10.1145/2503210.2503300>
- Day, S. M., Graves, R. W., Bielak, J., Dreger, D. S., Larsen, S., Olsen, K. B., ... Ramirez-Guzman, L. (2008). Model for basin effect on long-period response spectra. *Earthquake Spectra*, 24(1), 257–277. <https://doi.org/10.1193/1.2857545>
- Dreger, D. S., Beroza, G. C., Day, S. M., Goulet, C. A., Jordan, T. H., Spudich, P. A., & Stewart, J. P. (2015). Validation of the SCEC broadband platform v14.3 simulation methods using pseudospectral acceleration data. *Seismological Research Letters*, 86(1), 39–47. <https://doi.org/10.1785/0220140118>
- Field, E. H., & 2014 Working Group on California Earthquake Probabilities (2015). UCERF3: A new earthquake forecast for California's complex fault system: U.S. Geological Survey 2015–3009 (6 p.). <https://doi.org/10.3133/fs20153009>
- Frankel, A., Stephenson, W., & Carver, D. (2009). Sedimentary basin effects in Seattle, Washington: Ground-motion observations and 3D simulations. *Bulletin of the Seismological Society of America*, 99(3), 1579–1611. <https://doi.org/10.1785/0120080203>
- Goulet, C. A., Abrahamson, N. A., Somerville, P. G., & Wooddell, K. E. (2015). The SCEC broadband platform validation exercise: Methodology for code validation in the context of seismic-hazard analyses. *Seismological Research Letters*, 86(1), 17–26. <https://doi.org/10.1785/0220140104>
- Graves, R., & Pitarka, A. (2015). Refinements to the Graves and Pitarka (2010) broadband ground-motion simulation method. *Seismological Research Letters*, 86(1), 75–80. <https://doi.org/10.1785/0220140101>
- Graves, R., & Pitarka, A. (2016). Kinematic ground-motion simulations on rough faults including effects of 3D stochastic velocity perturbations. *Bulletin of the Seismological Society of America*, 106(5), 2136–2153. <https://doi.org/10.1785/0120160088>
- Graves, R. W., Aagaard, B. T., Hudnut, K. W., Star, L. M., Stewart, J. P., & Jordan, T. H. (2008). Broadband simulations for Mw 7.8 Southern San Andreas earthquakes: Ground motion sensitivity to rupture speed. *Geophysical Research Letters*, 35, L22302. <https://doi.org/10.1029/2008GL035750>

- Graves, R. W., & Pitarka, A. (2010). Broadband ground-motion simulation using a hybrid approach. *Bulletin of the Seismological Society of America*, 100(5A), 2095–2123. <https://doi.org/10.1785/0120100057>
- Graymer, R. W., Ponce, D. A., Jachens, R. C., Simpson, R. W., Phelps, G. A., & Wentworth, C. M. (2005). Three-dimensional geologic map of the Hayward Fault, Northern California: Correlation of rock units with variations in seismicity, creep rate, and fault dip. *Geology*, 33(6), 521–524. <https://doi.org/10.1130/G21435.1>
- Harmsen, S., Hartzell, S., & Liu, P. (2008). Simulated ground motion in Santa Clara Valley, California, and Vicinity from $M \geq 6.7$ scenario earthquakes. *Bulletin of the Seismological Society of America*, 98(3), 1243–1271. <https://doi.org/10.1785/0120060230>
- Johansen, H., Rodgers, A., Petersson, N. A., McCallen, D., Sjogreen, B., & Miah, M. (2017). Toward exascale earthquake ground motion simulations for near-fault engineering analysis. *Computing in Science & Engineering*, 19(5), 27–37. <https://doi.org/10.1109/MCSE.2017.3421558>
- Kamai, R., Abrahamson, N., & Graves, R. (2014). Adding fling effects to processed ground-motion time histories. *Bulletin of the Seismological Society of America*, 104(4), 1914–1929. <https://doi.org/10.1785/0120130272>
- Kim, A., Dreger, D. S., & Larsen, S. (2010). Moderate earthquake ground-motion validation in the San Francisco Bay Area. *Bulletin of the Seismological Society of America*, 100(2), 819–825. <https://doi.org/10.1785/0120090076>
- Krischer, L., Megies, T., Barsch, R., Beyreuther, M., Lecocq, T., Caudron, C., & Wassermann, J. (2015). ObsPy: A bridge for seismology into the scientific Python ecosystem. *Computational Science & Discovery*, 8(1), 14,003–14,020. <https://doi.org/10.1088/1749-4699/8/1/014003>
- Larsen, S. C., Dreger, D., Antolik, M., & Stidham, C. (2000). 3-D simulations of scenario earthquake along the Hayward fault, Technical Report UCRL-ID-137645 (8 p.). Lawrence Livermore National Laboratory.
- Lee, S. J., Komatitsch, D., Huang, B. S., & Tromp, J. (2009). Effects of topography on seismic wave propagation: An example from northern Taiwan. *Bulletin of the Seismological Society of America*, 99(1), 314–325. <https://doi.org/10.1785/0120080020>
- Olsen, K. B., Day, S. M., Minster, J. B., Cui, Y., Chouasia, A., Moore, R., ... Jordan, T. (2008). TeraShake2: Simulation of $M_w 7.7$ earthquakes on the southern San Andreas fault with spontaneous rupture description. *Bulletin of the Seismological Society of America*, 98(3), 1162–1185. <https://doi.org/10.1785/0120070148>
- Peter, D., Komatitsch, D., Luo, Y., Martin, R., Le Go, N., Casarotti, E., ... Tromp, J. (2011). Forward and adjoint simulations of seismic wave propagation on fully unstructured hexahedral meshes. *Geophysical Journal International*, 186(2), 721–739.
- Petersson, N. A., & Sjogreen, B. (2012). Stable and efficient modeling of anelastic attenuation in seismic wave propagation. *Communications in Computational Physics*, 12(1), 193–225. <https://doi.org/10.4208/cicp.201010.090611a>
- Petersson, N. A., & Sjogreen, B. (2014). Super-grid modeling of the elastic wave equation in semi-bounded domains. *Communications in Computational Physics*, 16(4), 913–955. <https://doi.org/10.4208/cicp.290113.220514a>
- Petersson, N. A., & Sjogreen, B. (2015). Wave propagation in anisotropic elastic materials and curvilinear coordinates using a summation-by-parts finite difference method. *Journal of Computational Physics*, 299, 820–841. <https://doi.org/10.1016/j.jcp.2015.07.023>
- Petersson, N. A., Sjogreen, B., & Rodgers, A. J. (2017). Full waveform modeling with mesh refinement in SW4 (abstract). Seismological Society of America Annual Meeting, Denver, CO, April 18–20, 2017
- Rodgers, A., Petersson, N. A., Nilsson, S., Sjogreen, B., & McCandless, K. (2008). Broadband waveform modeling of moderate earthquakes in the San Francisco Bay Area and preliminary assessment of the USGS 3D seismic velocity model. *Bulletin of the Seismological Society of America*, 98(2), 969–988. <https://doi.org/10.1785/0120060407>
- Sjogreen, B., & Petersson, N. A. (2012). A fourth order accurate finite difference method for the elastic wave equation in second order formulation. *Journal of Scientific Computing*, 52(1), 17–48. <https://doi.org/10.1007/s10915-011-9531-1>
- Taborda, R., & Bielak, J. (2013). Ground-motion simulation and validation of the 2008 Chino Hills, California, earthquake. *Bulletin of the Seismological Society of America*, 103(1), 131–156. <https://doi.org/10.1785/0120110325>
- Topozada, T. R., Brannum, D. M., Reichle, M. S., & Hallstrom, C. L. (2002). San Andreas fault zone, California; $M \geq 5.5$ earthquake history. *Bulletin of the Seismological Society of America*, 92(7), 2555–2601. <https://doi.org/10.1785/0120000614>
- United States Geologic Survey (2017). 3-D geologic and seismic velocity models of the San Francisco Bay Region. Retrieved from <https://earthquake.usgs.gov/data/3dgeologic>, last accessed December 30, 2017.
- Wessel, P., Smith, W. H. F., Scharroo, R., Luis, J. F., & Wobbe, F. (2013). Generic Mapping Tools: Improved version released. *Eos, Transactions American Geophysical Union*, 94(45), 409–410. <https://doi.org/10.1002/2013EO450001>
- Yu, E., & Seagall, P. (1996). Slip in the 1868 Hayward earthquake from the analysis of historical triangulation data. *Journal of Geophysical Research*, 101(B7), 16,101–16,118. <https://doi.org/10.1029/96JB00806>